Solute Transport in the Unsaturated Zone – an Experimental Approach

L. Badi, L. Zhuang and A. Raoof
Dep. of Earth Sciences, Utrecht University, Utrecht, the Netherlands

Abstract

Human activities cause release of various sort of chemical and contaminants at the earth surface. How these contaminants flow downwards in soil towards our underlying subsurface reservoirs is a serious and critical issue. This knowledge is needed for remediation of the contaminated soils as well as soil usage management. Therefore, transport of solutes into the top soil layer, which is an unsaturated zone, is the aim of this study. Here, we used the multistep-flux transport (MS-T) approach to measure solute dispersivity as a function of saturation, complemented with the gamma-ray transmission method to measure the breakthrough (i.e., arrival time) curves of pulse-injected solutes. Our set-up consists of a small column (3cm by 3cm by 2cm) containing a sand sample. The results of the ADE-model show that our porous medium has a saturated dispersivity of around 0.3-0.5 cm. The unsaturated dispersivity increases with decreasing saturation to a maximum of 1.54 cm (at Sw = 0.51). The dispersivity value then begins to decrease until it gets to 0.283 cm (at Sw = 0.28). We have established a relationship between dispersivity and soil water saturation, which is in agreement with some previous studies (Toride et al., 2003; Raoof and Hassanizadeh, 2013), while it is in disagreement with some others (Maciejwski (1993) and Kanzari et al. (2015)). The MIM-model has a similar trend to the ADE-model, however dispersivity starts to decrease at a higher saturation with respect to ADE (0.60 to 0.51) and generally has lower dispersivity values. This research confirms the presumption that dispersivity decreases beyond a certain critical saturation level.

Introduction

Air-water systems have a significant impact on natural systems such as unconfined groundwater aquifers, which are close to the surface. Since not only water, but viruses, colloids and dissolved contaminants are also capable of entering the ground, understanding the hydraulic properties of unsaturated soil so as to be able to model water flow and solute transport processes is essential.

Knowledge of the hydraulic properties of unsaturated soil is essential for us to be able to model water flow and solute transport processes and to acquire a deeper understanding of the latter. The investigation of solute transport in unsaturated conditions requires us to look deeper into the impact of changing water content (θ) on solute transport.

The saturation of a soil is defined as the amount of fluid (water) that is present in the soil pores compared to the gas phase and can take a value ranging from 0 to 1. A value of 1 represents fully saturated soils, and any value lower than 1 represents unsaturated soil. The key factor influencing transport of solutes in soils is dispersion. Dispersion represents the deviation of a solute from the mean displacement as a function of irregularities in the flow paths of the fluid. The advection-dispersion equation (ADE) for homogeneous soil and conservative solute, accurately describes the hydrodynamic dispersion in one dimension (Bear and Cheng, 2010);

$$D\frac{\partial^2 c}{\partial z^2} - v\frac{\partial c}{\partial z} = R\frac{\partial c}{\partial t} \qquad [1]$$

where D is the hydrodynamic dispersion coefficient [$L^2\ T^{-1}$], c the solute concentration [$M\ L^{-3}$], z the (downward) direction of flow [L], v the pore-water flow velocity [$L\ T^{-1}$] ($v = q/\theta_s$, q is the Darcy flux and θ_s is the saturated water content (porosity)), R the retardation factor [-] and t is the time [T]. The first term $\left(\frac{\partial^2 c}{\partial z^2}\right)$ describes the concentration change by hydrodynamic dispersion as a deviation of the second term $\left(\frac{\partial c}{\partial z}\right)$. The degree of dispersion is a function of average flow velocity and saturation of the porous medium, and this degree is linearly related to velocity for saturated porous media (Bear and Cheng, 2010).

$$D(v) = D_e + \alpha v \qquad [2]$$

where D is the dispersion coefficient [L2 T^{-1}], D_e the effective diffusion coefficient [L^2 T^{-1}], α the dispersivity [L] and v the velocity [L T^{-1}]. However, to account for the volumetric water content of the porous medium, the dispersion coefficient must be written as a function of both water content (θ) and velocity (v);

$$D(v,\theta) = D_e(\theta) + \alpha(\theta)v \qquad [3]$$

The contribution of molecular diffusion to the total dispersion coefficient is usually negligible for most flow velocities. It can become important however, at lower flow velocity conditions. The main principles of groundwater flow are provided in Appendix A.

To this date, the relation between unsaturated porous media and hydrodynamic dispersion has not been properly validated. Past researches have indicated the different relationships between the saturation of a porous medium and its dispersivity (Maciejewski, 1993; Maraqa et al., 1997, Padilla et al., 1999; Toride et al. 2003; Kanzari et al., 2015). Maciejewski (1993) found an inverse linear relationship between the dispersivity and saturation. Maciejewski (1993) and Kanzari et al. (2015) both indicate an increasing dispersivity with decreasing saturation. Toride et al. (2013) also showed this trend, however with dispersivity decreasing beyond a certain saturation. Padilla et al. (1999) found that dispersivity is not only a function of properties of the medium but also of its water content.

The symmetry of the breakthrough curve (BTC) shows significant changes when desaturating the porous medium in past literature (Krupp and Elrick, 1968; Gupta et al, 1973; Maraqa et al., 1997; Nützmann et al. 1998; Toride et al., 2003). Unsaturated hydrodynamic dispersion through porous media depends on many factors and therefore the literature study has found several different results. Tailing, which causes the shape of the BTC to change at the falling limb (and extends the length of the BTC), indicates that there are larger heterogeneities in the flow field as opposed to flow in saturated media (De Smedt and Wierenga, 1984; Kartha and Srivastava, 2008). At the top of the rising limb, a flattening of the curve is noticed. This was first recognized with a glass bead experiment by De Smedt and Wierenga (1984). They found that changes during unsaturated flow indicate a higher hydrodynamic dispersion.

There are several multistep approaches performed and described in previous studies. The multistep-outflow (MS-O) method was the first approach found for measuring the hydraulic properties of porous media, and is described in van Dam (1994), Zurmühl and Durner (1998) and Hopmans (2012). This method has recently been extended to the Multistep-flux method (MS-F), which is based on vertically uniform flow (Weller et al., 2011; Weller and Vogel, 2012). The Multistep Flux (MSF) approach is an ideal setup for measuring solute breakthrough curves (BTCs) and quantifying transport properties. This approach can measure BTCs at a constant h and uniform θ for different flow rates. However, in Kumahor et al. (2014) the MS-O and MS-F were combined with the Multistep-Transport (MS-T) approach that measures BTCs at constant pressure head and uniform water content for different flow rates. Notably, Maciejewski (1993) found the use of radiometric methods (gamma-ray transmission method) to be applicable for measuring saturation, and solute transport in soil.

In this study, we used the multistep-flux (MS-T) approach to measure solute dispersivity as a function of saturation under well-defined conditions (i.e. uniform gradient flow and uniform water content) so as to obtain a comprehensive data set for parameterizing unsaturated flow and transport processes in a consistent way. We carried out experiments using a small column with a sand sample to measure dispersivity as a function of saturation. The dimensions of the column are 3 cm (height) by 3 cm (length) by 2 cm (width). The approach is demonstrated for sand (0.1-0.5 mm) and complemented by using the gamma-ray transmission method to find the water content and the breakthrough curves of the pulse-injected solutes. The resulting data will be compared to the existing literature on saturation dependent dispersivity by the previously mentioned authors, to validate the conclusion of the experiments. This study aims to provide an increased understanding of dispersivity, and to investigate saturation-dependent solute transport. The research will also provide us with new insights on the use of gamma-ray for obtaining BTC's of solute flow.

Materials and Methods

Sand Material

The type of sand used during the experiments was obtained from a sand mining site (Sibelco) with particles ranging from 0.1 – 0.5 mm. The sand was rinsed with deionized water and then air dried before usage. The saturated hydraulic conductivity of the sample has already been obtained using a constant-head method (Reynolds et al., 2002). The properties of the sand are shown in table 1. These were described and given by Zhuang et al., (2017). The water retention curves of the sand were also provided in this paper.

Table 1. Properties of the sand used in the experiments (Zhuang et al., 2017)

Properties	**Values**
Mean particle diameter (d_{50}) mm	0.20
Uniformity coefficient (C_u)	2.3
Particle density (ρ_s) g cm^{-3}	2.56
Saturated conductivity (K_s) cm h^{-1}	61.2
Average porosity (φ)	0.39
C_u is the ratio of d_{60} to d_{10}	

Experimental set-up

Figure 1. Schematic view of the experimental setup for the multistep flux (MSF) experiments (Zhuang et al., 2017)

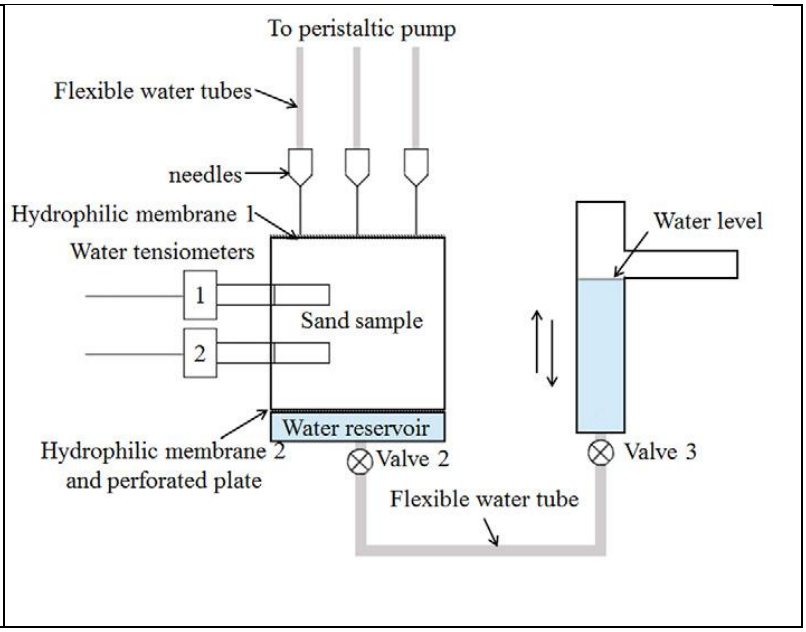

In figure 1, a schematic overview of the MSF experimental setup is shown. It is the same set-up as described by Zhuang et al., 2017. It consisted of a Plexiglas cell with dimensions of 3 cm (height) by 3 cm (length) by 2 cm (width). The Plexiglas was filled with the sand sample. At the bottom of the cell, a 5-mm hydrophilic nylon membrane was placed which was held by a stainless-steel porous plate to serve as a capillary barrier. The water

reservoir, positioned at the bottom of the setup was connected to a hanging water column (HWC), which was used to control the pressure head at the outlet. During drainage water flows out of the HWC.

Two tensiometers were installed at depths of 1 and 2 cm in the sand sample cell. They consisted of a ceramic cup, 1 cm long and 4 mm in diameter, and a small pore pressure transducer. Prior to use, the tensiometers were saturated with deionized water. To ensure that he tube between the ceramic cup and the transducer remained filled with water, a plastic syringe was used to connect the ceramic cup to a vacuum to remove air from the tensiometers (Zhuang et al., 2017).

The setup of the experiment also consisted of six injection needles (two in the lateral direction and three in the longitudinal direction) to obtain a spatially uniform water inflow rate to the top of the cell. The six needles were connected to tubes and those were connected to a peristaltic pump that controlled the injected flow rate. The saturated conductivity (*Ks*) of the sand used during the experiments has a value of 61.2 cm h^{-1} (see table 1). More information regarding the set-up has been provided in Appendix B.

Gamma-ray Transmission method

During the experiments, a gamma-ray transmission method is used. Gamma radiation consists of high-energy photons. When a beam of gamma radiation passes through a sample of thickness x, the transmission of photons can be described using the Beer-Lambert law. In case of an unsaturated soil sample, this law can be written as:

$$I = I_0 \exp(-\mu_s x_s - \mu_w x_w) \qquad [4]$$

where I is the measured intensity, I_0 the corresponding reference intensity, μ_s and μ_w are the soil and water attenuation coefficient, and x_s and x_w are the path lengths of the γ-ray beam through soil and water (Zhuang et al., 2017). How the attenuation coefficients were determined can be found in Appendix C. From the two radioactive sources, Cesium-137 and Americium-241, Americium is the more stable one because of the lower energy compared to Cs, and therefore has a higher accuracy (Zhuang et al., 2017). For this reason, only Am was emitted during the measurements. The values of the porosity (φ) of the sand and its water content (θ) can be calculated from x_s and x_w, using the following equations;

$$\varphi = \frac{x - x_s}{x} \quad \text{and} \quad \theta = \frac{x_w}{x} \qquad [5]$$

In the paper of Udagani (2013) a method is described to estimate the dependence of linear and mass attenuation coefficients of gamma rays on concentration of Manganese (II) chloride ($MnCl_2$). Based on their results, $MnCl_2$ is therefore used as a solute to inject in the column. A solution with 14% concentration (mass on mass ratio) will be injected. In Appendix C, the calibrations are provided of the attenuation coefficients and their differences in values when either Cs and Am are emitted, or when only Am was used. The measurement of saturation using *y*-ray can be found in Appendix D.

Data Analysis

For the analysis of the data acquired through experiments, we will use the STANMOD-CXTFIT program. This provides a clear estimate of the pore-water velocity and hydrodynamic dispersion coefficient. The pore-water velocities were measured during the experiment. Results are based on the fitted pore-water velocity value.

Advection-dispersion model and Mobile-immobile model

The advection-dispersion transport model (ADE) is applied to model the experimental data. Equation 1, given in the introduction, simulates the spread of solutes based upon advection and hydrodynamic dispersion as well as retardation due to partitioning of solutes between solid and fluid phase in a one-dimensional line. During this experiment we used a conservative tracer, therefore retardation was neglected. Since the sand has been packed as consistently as possible, using the same packing method as described by Zhuang et al, 2017, we can assume that there were isotropic and homogenous conditions in the porous medium, although the flow domain is three-dimensional. The ADE model is sufficiently accurate for a relatively high mobile water content (Raoof and Hassanizadeh, 2013). However, in unsaturated soils with a lower saturation, the ADE analytical solution may not be accurate enough because of the different conditions that may arise. Therefore, the Mobile-Immobile model (MIM-model) was applied. The initial conditions for the MIM-model are similar to the ADE-model. However, MIM also requires initial conditions for the partitioning between the mobile and immobile regions, β [-], as well as first-order transfer coefficient between the two regions, ω [T^{-1}]. This has been described more in detail by de Witte (2017).

Results and Discussion

The experiments have been performed for primary drainage. The level of the hanging column was kept lower than the tensiometers readings during drainage. During the flow experiments a solution of 14% w/w $MnCl_2$ was injected at various levels of saturation to obtain the breakthrough curves. For each saturation level the two tensiometers readings were observed. Once the difference between the two tensiometers reached values close to zero and were stabilized, thus reflecting steady-state conditions, the solution can be injected.

Unsaturated hydraulic conductivity

The unsaturated hydraulic conductivity was calculated using the van Genuchten-Mualem model which is based on the pore size distribution model of Mualem (Fritz, 2012);

$$k_{rw} = \sqrt{S_e}\left[1 - \left(1 - S_e^{\frac{1}{m}}\right)^m\right]^2 \qquad [6]$$

where k_{rw} is the relative permeability of the wetting phase, S_e is the effective saturation (equation for S_e is provided in Appendix A3.1), m is related to n by $1-\frac{1}{n}$, where n accounts for the uniformity of the porous medium. The value of n has been extracted from Zhuang et al. (2017). The resulting k_{rw} is multiplied with K_s, to determine the flow velocity of the pump for each saturation level. These equations have been further described by Fritz (2012).

Analysis of experimental data

Modelling by Advection-Dispersion model

The BTC's in figures 2, 3 and 4 show the results from the experiments at different saturation of the porous medium. For all breakthrough curves, the concentration has been normalized to the maximum concentration (concentration of influent $MnCl_2$-solution) as follows:

$$C_n = \frac{C - C_0}{C_1 - C_0} \qquad [8]$$

where C_n is the normalized concentration [-], C is the measured concentration [M L^3], C_1 is the input concentration [M L^3], and C_0 is the initial concentration [M L^3].

Table 2. ADE-model results from unsaturated transport experiments for porous medium							
S_w [-]	*θ* [-]	*q [cm min^{-1}]*	*v [cm min^{-1}]*	*D [cm^2 min^{-1}]*	*α_m [cm]*	*r^2*	*Pc [Pa]*
1.0	0.39	2.615	2.685	1.370	0.510	0.990	0
1.0	0.39	1.308	1.259	0.358	0.284	0.944	0
0.78	0.312	1.103	1.069	0.758	0.709	0.935	32.4
0.69	0.273	0.664	0.664	0.661	0.996	0.977	34.1
0.60	0.234	0.365	0.378	0.530	1.404	0.972	35.6
0.51	0.195	0.163	0.112	0.172	1.540	0.940	37.2
0.41	0.156	0.100	0.075	0.088	1.167	0.908	39.1
0.28	0.117	0.025	0.023	0.006	0.283	0.900	42.2

Table 2 shows the results from modelling saturated and unsaturated flow experiment data with the ADE-model through the porous media. This includes the volumetric water content (θ), the Darcy flux (q, calculated by dividing the velocity of the pump by porosity), the (mobile phase) velocity v (result of CXTFIT), the (mobile phase) dispersion coefficient (D), the coefficient of determination (r^2), capillary pressure (Pc). Both velocity and dispersion coefficient represent an average value for the entire flow domain for each saturation at 1.5 cm from the flow inlet. The capillary pressure has been determined using Equation 9.

$$p_c(S_e) = \frac{1}{\alpha}\left(S_e^{-\frac{1}{m}} - 1\right)^{\frac{1}{n}} \text{ for } p_c > 0 \qquad [9]$$

where α is the invert of pressure (1/Pa) (Fritz, 2012). The definition of the other parameters can be found in the description of equation 6 and 7. We used the calculation of the capillary pressure to estimate the position of the HWC in our set-up (see figure 1).

Figure 2. Breakthrough curves under saturated condition (S_w=1) at one location (1.5 cm) from inlet. q_1 = 2.685 cm min^{-1} and q_2 = 1.259 cm min^{-1}. Points indicate observation data, lines indicate fit by ADE-model in CXTFIT and MIM-model

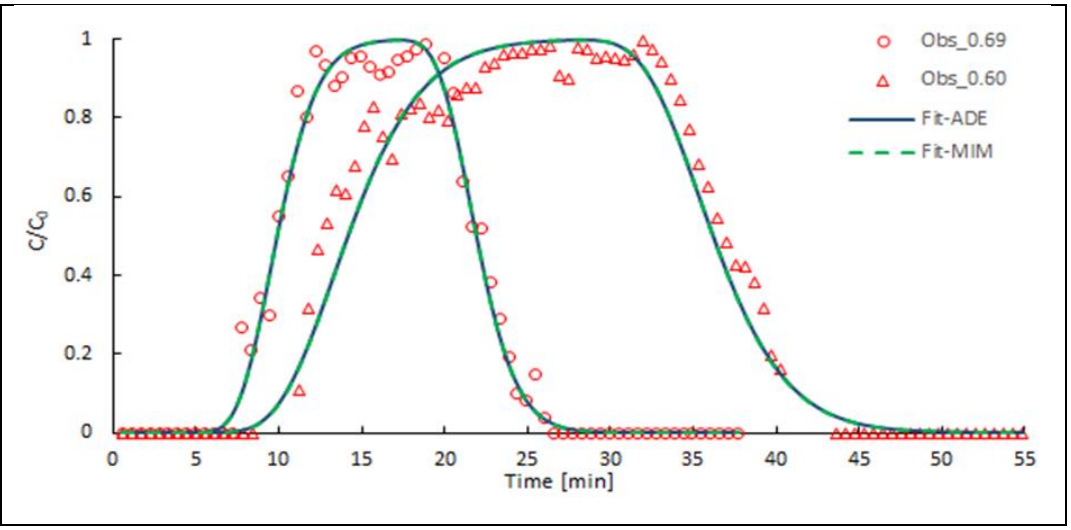

Figure 2 displays the breakthrough curves for two velocities (q_1 = 2.685 cm min^{-1} and q_2 = 1.259 cm min^{-1}) for the saturated porous medium. The graphs show a Gaussian distribution, indicating that there are few irregularities in the flow paths and a high

mobile water content. Both are shown to have dispersivity values similar to each other (table 2), showing that the sand in the column is distributed quite homogeneous. There is a small difference in the maximum concentration, which could have been caused by either the accuracy of the gamma-ray (Appendix C), or it has not reached its maximum concentration yet. Interestingly, however, is that the dispersivity increases slightly with increased flow velocity.

Figure 3. Breakthrough curves under unsaturated condition (S_w=0.69 and 0.6) at one location (1.5 cm) from inlet. q_1 (S_w = 0.69) = 0.664 cm min^{-1} and q_2 (S_w = 0.60) = 0.378 cm min^{-1}. Points indicate observation data, lines indicate fit by ADE-model in CXTFIT and MIM-model

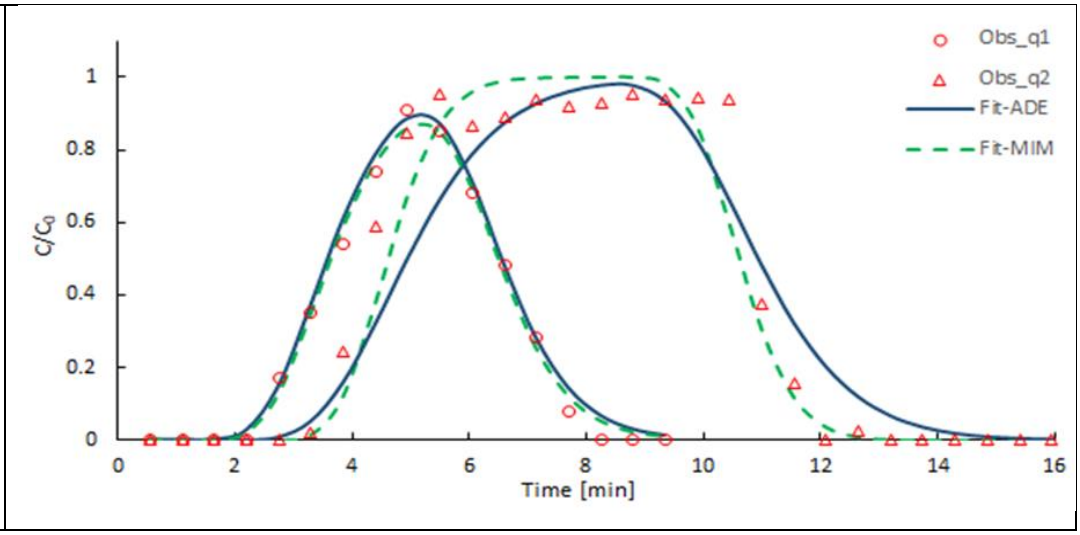

Figure 4. Breakthrough curves under unsaturated condition (S_w=0.41 and 0.28) at one location (1.5 cm) from inlet. q_1 (S_w = 0.41) = 0.075 cm min^{-1} (left) and q_2 (S_w = 0.28) = 0.023 cm min^{-1} (right). Points indicate observation data, lines indicate fit by ADE-model in CXTFIT and MIM-model

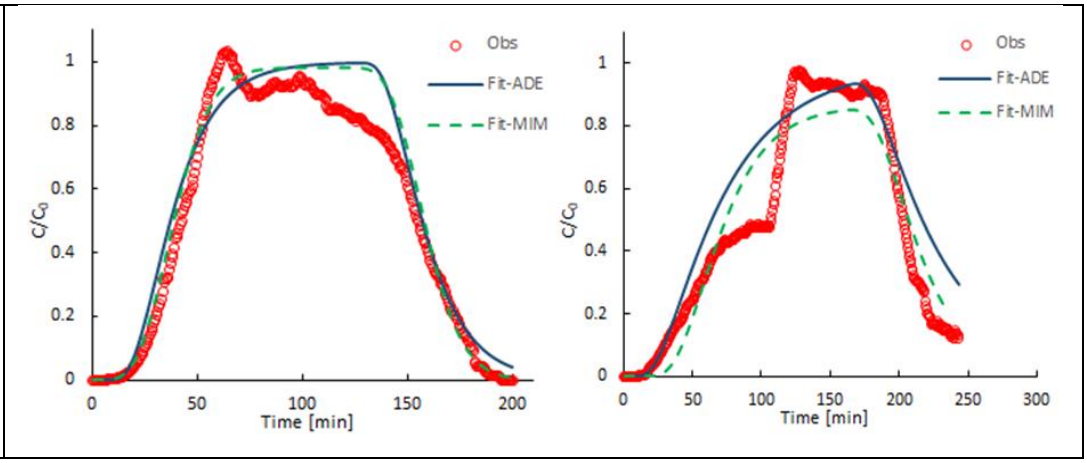

The breakthrough curves shown in figure 3 and 4, show a different concentration profile than for the saturated condition in figure 2. The shape of the breakthrough curve shows signs of immobile water content and a higher dispersion coefficient. In the rising limb of the breakthrough curve a flattening near the top can be seen. Whereas in the falling limb, there is evidence of tailing. There are some deviations shown in comparison to the fitted curves, such as in figure 4 (S_w = 0.28) from t = 125 min to t = 170 min, which most likely is affected by the heterogeneities in the column. As shown in figure 3, the breakthrough curve for a S_w = 0.60 shows a large effect of dispersion to the concentration distribution

over time. Table 2 shows an increase in dispersivity values when decreasing the saturation. As water content decreases, the pore-water velocity decreases and the geometry of the liquid phase in water-conducting pores changes with less opportunity for mixing and increased tortuosity. The dispersion coefficient will depend on both water content and velocity, as seen in equation 3. Therefore, an increase of dispersivity can be explained due to those factors, as there is less volume to disperse in.

However, for $S_w < 0.41$, the dispersivity decreases again. In low saturation of a porous medium, micropore flow becomes the dominant flow regime instead of the macropore flow in the displacement of fluids. Inside the smaller pore spaces, there is higher capillary interaction with the solids. Pores are therefore able to retain water, however, the flow through these pores remains transient. Since flow is limited to generally fewer flow paths, the variation in flow becomes less significant. These factors influence the total dispersion coefficient for a specific saturation. These results seem to be complementary to the results of Toride et al., 2003 and Raoof and Hassanizadeh, 2013. As in these researches, they have found a similar trend in the dispersivity, the rising limb and the falling limb with decreasing saturation.

Modelling by Mobile-Immobile (MIM) model

Besides the results of the ADE-model, we also employ another model, namely the Mobile-Immobile (MIM) model. This can increase the accuracy of the model results from the ADE-model, which is the case for our results, when comparing the values of r^2. The Mobile-Immobile model considers a division in the mobile and immobile water content and applies an exchange parameter between the two regions. This will provide us two more parameters as a function of the saturation.

One is parameter β [-], and is defined as the mobile water content fraction.

$$\beta = \frac{\theta_m}{\theta} \qquad [10]$$

where θ is defined as $\theta_m + \theta_{im}$. The MIM assumes that the liquid phase in soil pores can be partitioned into mobile (flowing) and immobile (stagnant) regions; $\theta = \theta_m + \theta_{im}$.
The other parameter is the mass transfer coefficient, ω [min^{-1}]. The results of the MIM-model are provided in the figures 2,3 and 4, and in table 3. When speaking of the mass

transfer coefficient ω, Padilla et al. (1999) described that greater velocities enhance the mass transfer rates by causing faster mixing between the two regions.

However, there is not a clear trend visible in our results. Although we did find higher values of ω for lower saturation.

Table 3. MIM-model results from unsaturated transport experiments for porous medium

S_w [-]	θ [-]	*q [cm min^{-1}]*	*v [cm min^{-1}]*	*D [cm^2 min^{-1}]*	*α_m [cm]*	*B [-]*	*ω [min^{-1}]*	*r^2*	*Pc [Pa]*
1.0	0.39	2.615	2.684	1.368	0.510	0.998	1,53E-4	0.992	0
1.0	0.39	1.308	1.250	0.334	0.284	0.984	1,12E-3	0.956	0
0.78	0.312	1.103	1.114	0.580	0.709	0.949	1,00E-6	0.962	32.4
0.69	0.273	0.664	0.662	0.654	0.996	0.955	1,87E-3	0.986	34.1
0.60	0.234	0.365	0.375	0.531	1.404	0.922	1,00E-6	0.973	35.6
0.51	0.195	0.163	0.101	0.131	1.540	0.852	3,35E-2	0.980	37.2
0.41	0.156	0.100	0.046	0.022	1.167	0.754	6,47E-2	0.945	39.1
0.28	0.117	0.025	0.021	0.007	0.283	0.937	3,43E-2	0.908	42.2

Interestingly, as seen in the figures above, is that there is a large difference in the fitted curves of ADE and MIM model for the saturated condition of q_2. This is also seen, for S_w = 0.28, where the difference between the fitted curves are also more visible, but have improved in the case of the MIM-model. This might be due to do the added parameters, which makes the fit for these cases more accurate to the observed data points. In case of the other BTC's, the difference in the MIM-fit is much smaller with respect to ADE.

However, the dispersivity of the MIM-model for the mobile region increases with decreasing saturation up to a saturation of 0.60, whereas the ADE-model has a peak dispersivity at a saturation of 0.51 (see figure 5). A possibility is that there is a difference in dispersive behaviour between the models. However, de Witte (2017) has found a reverse situation in his research, where the MIM-model start its decrease at a lower saturation with respect to ADE.

Generally, the dispersivity of the MIM-model has lower values than the ADE model. This is likely due to the added parameters, in which the model takes the division into account of mobile and immobile water portions.

Figure 5. Modelled dispersivity (α) values over saturation (S_w)

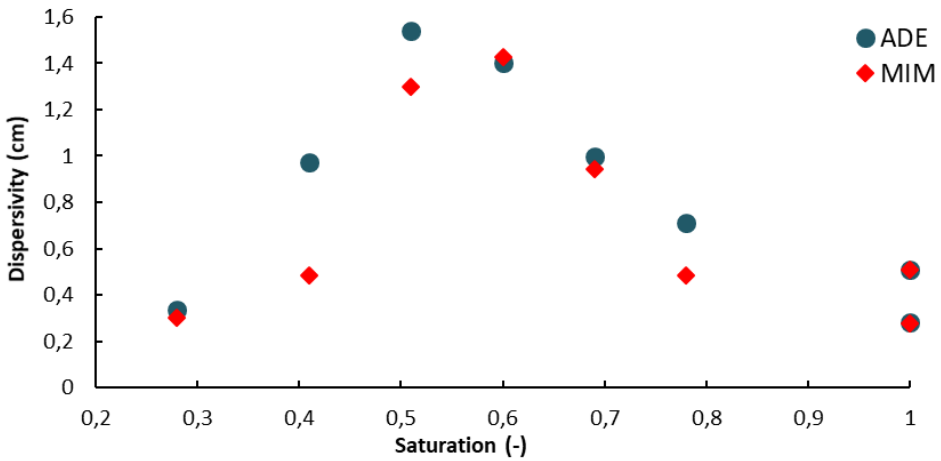

Figure 6. Mobile fraction [β] as a function of saturation [S_w]

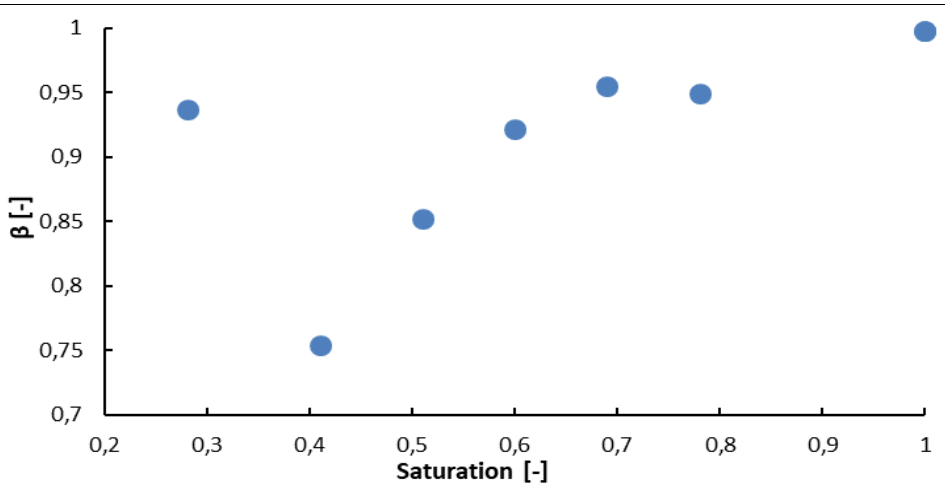

Figure 6 presents the mobile fraction as a function of saturation (S_w). With decreasing saturation, the mobile water content only decreases. The amount of stagnant water zones is therefore larger in a low-saturation flow domain, according to the MIM model output. However, in very low saturation conditions, such as 0.28, a greater β value is found. This can be explained due to the relative water mobility. On average, the water in the column reaches a very low mobility, relative to each other however, they have the same mobility. Therefore implying, a high mobility fraction (Toride et al, 2003).

Conclusion

For this study we measured solute dispersivity under a range of soil saturation values to obtain a comprehensive data set to parameterize unsaturated flow and transport processes in a consistent way. In pursuit of this, breakthrough curves of the solute pulse injections have been measured in an experimental column at various saturation levels. The concentration measurements have been performed using the gamma-ray, as a newly described method. The obtained data of the concentration as a function of time has been analytically processed using modelling software CXTFIT. This provides us with the dispersivity as a function of soil saturation.

The established relationship shows to be in agreement with previous studies (Toride et al., 2003; Raoof and Hassanizadeh, 2013). However, we have found a disagreement with the studies of Maciejwski (1993) and Kanzari et al. (2015), since they have found a linear relationship between dispersivity and saturation. A key finding of this research was the confirmation of the presumption that dispersivity decreases after a certain saturation.
The Advection Dispersion model shows that our porous medium has a saturated dispersivity of around 0.3-0.5 cm. The unsaturated dispersivity then increases with decreasing saturation to a maximum of 1.54 cm at a saturation of S_w = 0.51. After this saturation, the dispersivity decreases till a value of 0.283 cm at a saturation of S_w = 0.28. Lower saturation has not been possible to achieve, since residual saturation would be reached, at which point diffusion will be the dominant process of displacing solutes. The Mobile-Immobile model has a similar trend to the ADE model in terms of an increase of dispersivity towards an intermediate saturation. However, dispersivity starts to decrease at a higher saturation with respect to the ADE (0.60 to 0.51). Which is actually reverse to the findings of de Witte (2017). Overall, the dispersivity values also have lower values than the ADE-model, which is because the MIM-model takes the division into account of mobile and immobile water portions.

Further research is advised on finer and coarser porous media, to measure the characteristics of the particle sizes to dispersivity. Lower saturations should also be investigated to ensure and confirm with more certainty the decrease of dispersivity after a certain saturation. The hope is that this study will provide more insight in the mechanics of solute dispersion in unsaturated soils and improve estimation of dispersion in homogenous soils.

References

Barataud, F., Moyne, C. & Stemmelen, D., 1999. Measurement of Soil Water Diffusivity of an Undisturbed Forest Soil Using Dual-Energy Gamma Radiation Technique. *Soil Science*, 164(7), pp.493–502.

Bear, J., & Cheng, A. H. D. (2010). *Modeling groundwater flow and contaminant transport* (Vol. 23). Springer Science & Business Media.

Darcy, H. (1856). *Les fontaines publiques de la ville de Dijon: exposition et application…*. Victor Dalmont.

De Smedt, F. and Wierenga, P. J. (1984). Solute Transfer Through Columns of Glass Beads. Water Resources Research, 20(2):225–232.

Fritz, S (2012). Experimental investigations of water infiltration into unsaturated soil: Analysis of dynamic capillarity effects. M.S. thesis. Stuttgart Univ., Stuttgart, Germany.

Gupta, R., Millington, R., and Klute, A. (1973). Hydrodynamic dispersion in unsaturated porous media. I. Concentration distribution during dispersion. J. Indian Soc. Soil Sci., (21):1–7.

Hendriks, M. (2010). *Introduction to physical hydrology*. Oxford University Press.

Kanzari, S., Hachicha, M., and Bouhlila, R. (2015). Laboratory Method for Estimating Solute Transport Parameters of Unsaturated Soils Laboratory 1:149–154.

Kartha, S. A. and Srivastava, R. (2008). Effect of immobile water content on contaminant transport in unsaturated zone. Journal of Hydro-Environment Research, 1(3-4):206–215.

Krupp, H. and Elrick, D. (1968). Miscible displacement in an unsaturated glass bead media. Water Resources Research, (4):809–815.

Kumahor, S. K., de Rooij, G. H., Schlüter, S., & Vogel, H. J. (2015). Water flow and solute transport in unsaturated sand—a comprehensive experimental approach. *Vadose Zone Journal*, *14*(2).

Maciejewski, S. (1993). Numerical and experimental study of solute transport in unsaturated soils. Journal of contaminant hydrology, 14:193–206.

Maraqa, M. A.,Wallace, R. B., and Voice, T. C. (1997). Effects of degree of water saturation on dispersivity and immobile water in sandy soil columns. Journal of Contaminant Hydrology, 25(3-4):199–218.

Mualem, Y., 1976. A new model for predicting the hydraulic conductivity of unsaturated porous media. *Water Resources Research*, 12(3), pp.513–522.

Nützmann, G., Thiele, M., Maciejewski, S., and Joswig, K. (1998). Inverse modelling techniques for determining hydraulic properties of coarse-textured porous media by transient outflow methods. Advances in Water Resources, 22(3):273–284.

Padilla, I. Y., Yeh, T. C. J., and Conklin, M. H. (1999). The effect of water content on solute transport in unsaturated porous media. Water Resources Research, 35(11):3303–3313.

Reynolds, W. D., Elrick, D. E., Youngs, E. G., Amoozegar, A., Booltink, H. W. G., & Bouma, J. (2002). 3.4 Saturated and field-saturated water flow parameters. *Methods of soil analysis, Part*, *4*, 797-801.

Stolte, J. (1997). Determination of the saturated hydraulic conductivity using the constant head method. Manual for soil physical measurements. Tech. Doc, 37, 27-32.

Toride, N., Inoue, M., and Leij, F. J. (2003). Hydrodynamic dispersion in an unsaturated dune sand. Soil Science Society of America Journal, 67(3):703–712.

Udagani, C. (2013). Dependence Of Gamma Ray Attenuation On Concentration Of Manganese (II) Chloride Solution. *International Journal Of Scientific & Technology Research*, *2*(7).

Witte, R. D. (2017). *Dispersivity-Saturation relationship for various porous media; Experiments and modelling* (Master's thesis).

Zhuang, L., Bezerra Coelho, C. R., Hassanizadeh, S. M., & van Genuchten, M. T. (2017). Analysis of the Hysteretic Hydraulic Properties of Unsaturated Soil. *Vadose Zone Journal*, *16*(5).

Appendix A

In the introduction, the main principles behind unsaturated transport have already been described. However, the basic processes of saturated transport, permeability and hysteresis are described to provide the context behind the method and results of the experiments.

1. Saturated transport principles

The saturated hydraulic conductivity (K_s) is an important parameter to predict soil water flow. It is determined by using a steady state constant head method based on Darcy's Law (equation 1). A constant water level is maintained on top of an undisturbed soil sample. The volume of water that percolates through the sample is measured over time (Stolte, 1997).

$$q = K\frac{dH}{dz} \quad [1]$$

Darcy's law can be rewritten to enable us to extract the saturated hydraulic conductivity of the sand;

$$K = \frac{V}{t_v Z}\frac{dH}{dz} \quad [2]$$

where K is the hydraulic conductivity [L^2 T^{-1}], V is the outflow volume [L^3], t_v is elapsed time during collection of outflow volume [T], A is the area of the column [L^2], dz is the height of the sand [L] and dH is the total hydraulic head over the height of the sand [L].

2. Permeability

Permeability can be divided into two categories; intrinsic permeability and relative permeability. The intrinsic permeability is the measure for the ease at which a fluid (water) can flow through a soil, which is the same definition as the hydraulic conductivity. However, for the hydraulic conductivity the properties of the fluid are also considered (as seen in equation 1.4), which is not the case of the intrinsic permeability.

Darcy's law (Darcy, 1856) describes the relation between the hydraulic conductivity and permeability as follows;

$$K = \frac{\kappa \rho g}{\mu} \quad [3]$$

where K is the hydraulic conductivity [L T^{-1}]; κ is the intrinsic permeability [L^2] and μ is the dynamic viscosity of the fluid [M L^{-1} T^{-1}].

The relative permeability is dependent on the saturation, since for a multiphase flow system in a porous medium the mobility of water is higher at a higher saturation. Therefore, the permeability needs to be corrected, because both phases (the wetting fluid and non-wetting fluid) impede the flow on the other phase (Mualem, 1976).

3. Capillary pressure and Hysteresis

3.1 Capillary pressure

The main property available for a porous medium is the porosity, which is the amount of void space. Saturation and capillary pressure are strongly correlated. The wetting phase tends to maximize its contact with the solid phase. In the experiments that will be performed, the non-wetting phase will replace the wetting phase. This implies that the largest pores will be entered first. Therefore, capillary pressure decreases with increasing saturation. Many models exist to describe the relationship of saturation and capillary pressure, mostly based on experimental data. One of the most famous models for two phase systems, is the van Genuchten model. With the model, the so-called soil water retention curves can be described where capillary pressure is related to the saturation of the wetting phase. The effective saturation Se of the wetting phase is defined as:

$$S_e(p_c) = \frac{S_w - S_{wr}}{1 - S_{wr}} \quad [4]$$

where S_w is the saturation of the wetting phase, S_{wr} is the residual saturation.

3.2 Hysteresis

In the porous medium, imbibition or drainage are important processes affecting the water content within the column. Imbibition occurs when a wetting fluid displaces a non-wetting fluid, which is the contrary to drainage, where a non-wetting phase displaces the wetting fluid. Only drainage will be applied during the experiments.

Multiphase flow behaviour in a porous medium in a current state is affected by the past events that took place in the porous medium. This implies that after each sequence of infiltration and drainage, the phases react differently. The van Genuchten model (equation 2.2-2.4) itself uses the pore size distribution model of Maulem (1976).

$$S_{ew} = [1 + (\alpha * P_c)^n]^{-m} \; for \; P_c > 0 \qquad [5]$$

m can be related to n by;

$$m = 1 - \frac{1}{n} \qquad [6]$$

Solving for P_c yields:

$$P_c(S_{ew}) = \frac{1}{\alpha}\left(S_{ew}{}^{-\frac{1}{m}} - 1\right)^{\frac{1}{n}} \; for \; P_c > 0 \qquad [7]$$

were *n* accounts for the slope of the curve. When n increases it leads to a flatter curve and a more uniform pore distribution. The coefficient α [Pa^{-1}] determines the shape of the graph at an effective saturation near 1. P_c is the capillary pressure, which is a changeable variable. These changes at different states are shown in figure 1, which is based on the model of van Genuchten.

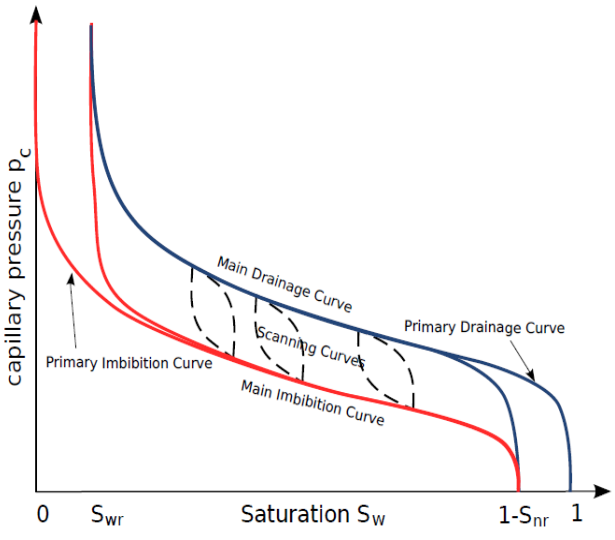

Figure 1: Hystersis model in Pc-S curve (Fritz, 2012)

If an experiment would start with a dry soil and water is infiltrated, the saturation will follow the primary imbibition curve until it reaches its maximum wetting saturation. This is indicated as $1\text{-}S_{rnw}$. This implies that the maximum saturation is the difference between full saturation (1) minus the residual saturation of the non-wetting phase (S_{rnw}). When higher capillary pressure would be applied on the sample, the saturation will follow the main drainage curve, since the wetting fluid would be replaced by the non-wetting fluid.

The scanning curves (indicated in the figure as the red lines), are followed when drainage or imbibition is stopped halfway. The curves will eventually reach the main curves again.

Several phenomena influence the process of hysteresis. Three phenomena are distinguished by Hendriks (2010):

- **Ink Bottle effect:** Pores that are shaped like an ink bottle react in a different manner to imbibition or drainage. This is due to different drainage or filling thresholds of the wide and narrow parts of the pore.
- **Contact angle effect**: The contact angle of the wetting phase tends to be smaller in a draining soil when compared to a wetting soil. This causes a higher suction in a draining situation.
- **Entrapment of the wetting or non-wetting phase:** During drainage or imbibition, bubbles of air or pores of water become isolated. These bubbles or pores are now trapped and will not further take part in flow of the particular phase. This effect leads to residual saturation of both phases.

Appendix B

1. Hanging water column experiment

A well-known experimental approach to measure soil hydraulic properties is the multistep- outflow (MS-O) approach (see figure 1). This method has shown to be useful with providing valuable information on hydraulic nonequilibrium (Diamantopoulos et al, 2012). However, we extended this method to a multistep-flux (MS-F) approach (as seen in the paper).

In figure 1, a schematic overview of the HWC experimental setup is shown. It consists of the same elements as described in the paper, only without the needles, pump and flexible water tubes. The pressure transducers were connected to a CR1000 datalogger (Campbell Scientific). Tensiometers readings were collected every 30 seconds. The water contents in the middle of the sand sample were measured using the *y*-ray transmission method.

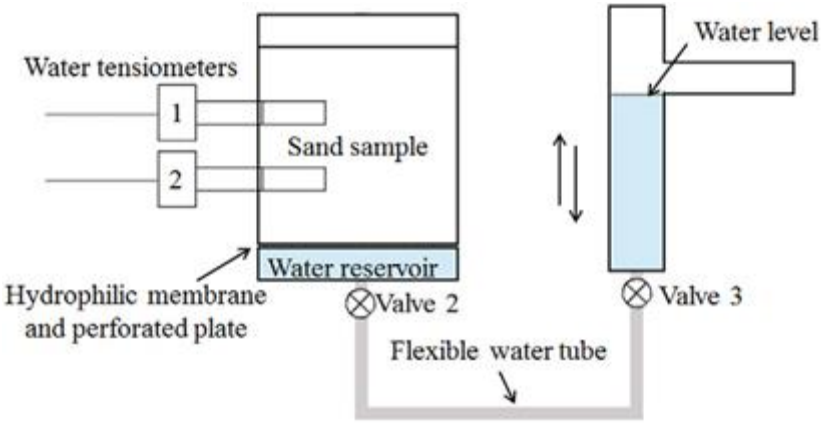

Figure 1: Schematic view of the experimental setup for the hanging water column (HWC) experiments (Zhuang et al.,2017).

2. Multistep Flux approach

The method of the Multistep Flux (MSF) was used during the experiments. In figure 2, a schematic view is provided of the experimental setup. This method allows measurements of $K(h)$ assuming unit gradient conditions during steady-state downward flow in a soil column, and the water retention curve can be measured directly. The water inflow rates are adjusted to achieve the same pressure heads when measured at two or more vertical positions. The fluid flow rate then becomes equal to K at the measured h. The measurements were repeated at various flow rates and corresponding pressure heads to produce the desired hydraulic data points (Zhuang et al., 2017).

Water flow in the porous medium was described using the standard Darcy-Buckingham equation:

$$q = -K(\theta)\left(\frac{\partial h}{\partial z} - 1\right) \quad [1]$$

were q is the fluid flux [L^2 T^{-1}] and z is vertical spatial coordinate. When there is unit gradient flow in the vertical direction, which implies $\partial h/\partial z = 0$, the flux becomes equal to the hydraulic conductivity, $K(h)$. Different hydraulic conductivity values are adjusting the inflow rate and h by changing the height of the hanging water column (Zhuang et al., 2017).

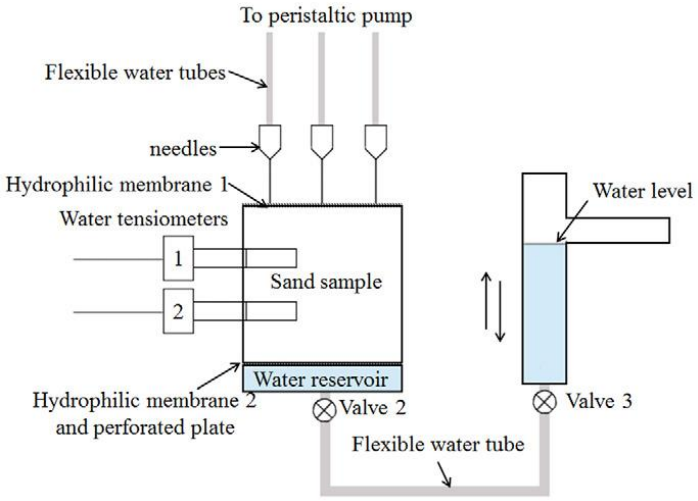

Figure 2. Schematic view of the experimental setup for the multistep flux (MSF) experiments

Pump

For saturation, K_s of the sand, as determined by Zhuang et al. (2017), is converted into cm min^{-1} to determine the value of the pump. This would have to equal a velocity of 1.02 cm min^{-1}. The pump has been calibrated, in order to find the appropriate value on the pump to each velocity. value on the pump equals the right velocity. The discharge of the flow is the velocity *Ks* divided by the porosity, which is 0.39 (q = v/n, where q is the discharge (cm min^{-1}), v is the velocity (cm min^{-1}) and n is the porosity (-). This yields a discharge of 2.62 cm min^{-1}.

Delay in arrival time solution

The set-up also consisted of tubes from the reservoirs, through the pump, to the six needles above the column. Therefore, an adjustment is made in the arrival time of the solute injection. The, what we call, the delay time, is calculated over the length of the tubes and the velocity of the flow. This calculated delay time is then subtracted from the measured time.

Appendix C

1. Attenuation coefficient

The attenuation coefficients have already been determined before the experiments. Details of the calibration procedures were given by Fritz (2012). A summary of those procedures will be described.

The linear attenuation coefficient (μ_w) of water corrects for the radiation that is attenuated by the water. This value differs for each source. The reference intensity (I_0) refers to the intensity of photons in the case of an absence of the material in the medium, for which the attenuation coefficient would apply. An example to clarify, would be the measurement of the saturation of sand. Before determining the value of I_0 the value of dry sand is measured first with the same sample thickness as when a substance is added. When adding the substance (water), the path length would represent the length that the gamma-beam travels through the substance (Zhuang et al., 2017).

During our calibration, the thicknesses of water depends on the placement of different number of cuvettes in a row. The attenuation coefficients of water, soil and the solution (further described in section …) has been calculated by using one to seven cuvettes. Since the thickness of the cuvettes used are 1 cm, the obtained measurements are from one to seven centimeters of water. The corresponding numbers of empty cuvettes were measured first to determine the initial intensities I_0. Using the Beer-Lambert equation (1) the attenuation coefficient for water can be determined.

Plotting the natural logarithm of the intensity of the measurements with water (I) divided by the reference intensities measurements (I_0) against the number of cuvettes (x) provides a linear graph (equation 3.5). The slope determines the attenuation coefficient (μ). Each measurement takes 30 seconds and is repeated three times to determine the accuracy. Fritz (2012) found the attenuation coefficient of both Americium and Cesium, of which the obtained value of Americium has a higher accuracy. We will provide our measurements of also both, and only Am, to determine the accuracy and with method we will apply during the experiments.

$$\ln\left(\frac{I}{I_0}\right) = -\mu x \qquad [1]$$

2. Compton scattering

When photons are emitted from the source, a collision might take place with a free electron in the detector. On this occasion, the photon loses energy and is scattered at a certain angle. When this loss of energy takes place, it means that photons of a gamma emitter of a higher energy (Cs) can enter the spectral field of the second emitter of lower energy (Am). Therefore, as described by Barataud et al., (1999) a correction is necessary to account for this effect. This will enable us to calculate the actual Americium intensity in case both Cs and Am are emitted.

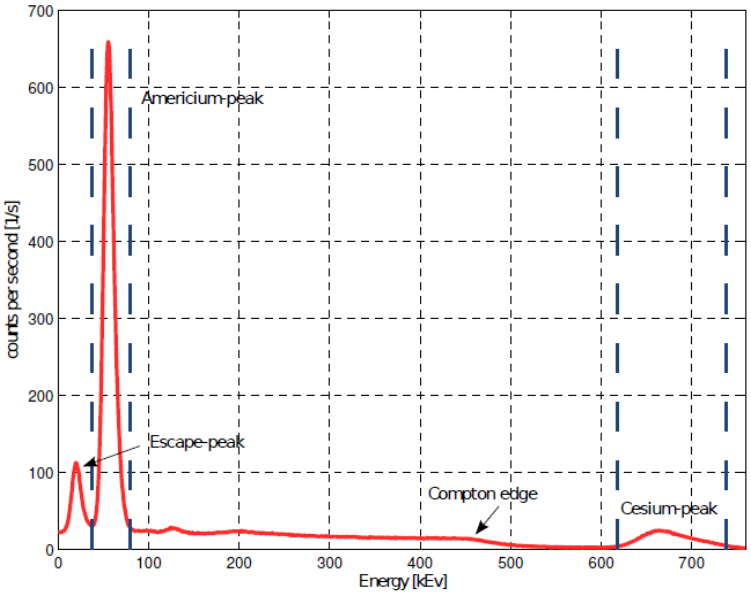

Figure 1: Characteristic curve for gamma radiation (Fritz, 2012).

The Compton edge, marked in the spectrograph of figure 1, is the maximum energy a photon can retain when it is slowed down by the electron. This is registered by the detector when the photon continues to move at an angle of 180 degrees. This Compton-effect can be corrected by performing a few measurements. As described by Fritz (2012) brass has a high adsorption of Americium compared to the adsorption of Cesium.

Using brass, it would be possible to differentiate between radiation from the Americium source and the Cesium source. The source of the gamma-ray is shielded with 1 mm thin piece of brass, where after every measurement another piece is added. In the procedure of Fritz (2012) they found that for 4 mm of Brass, 99 % of the Americium is adsorbed while only 20% of the Cesium gets adsorbed. The counts in the range of Americium energies are measured, which are now only caused by Compton scattering. This is further explained by Fritz (2012).

Important to note, is the effect of 'dead time' during measurements. This occurs when a photon with its specific energy is detected, and the detector cannot process and measure another photon. This leads to dead time. This however can be corrected by 'real time' measurements. These are measurements of the system when it automatically extends its measuring time, depending on the measured count rates. The higher the count rates the higher the dead times will be. The data of the measurement time will be shown as real time.

2.1. Results Compton scattering

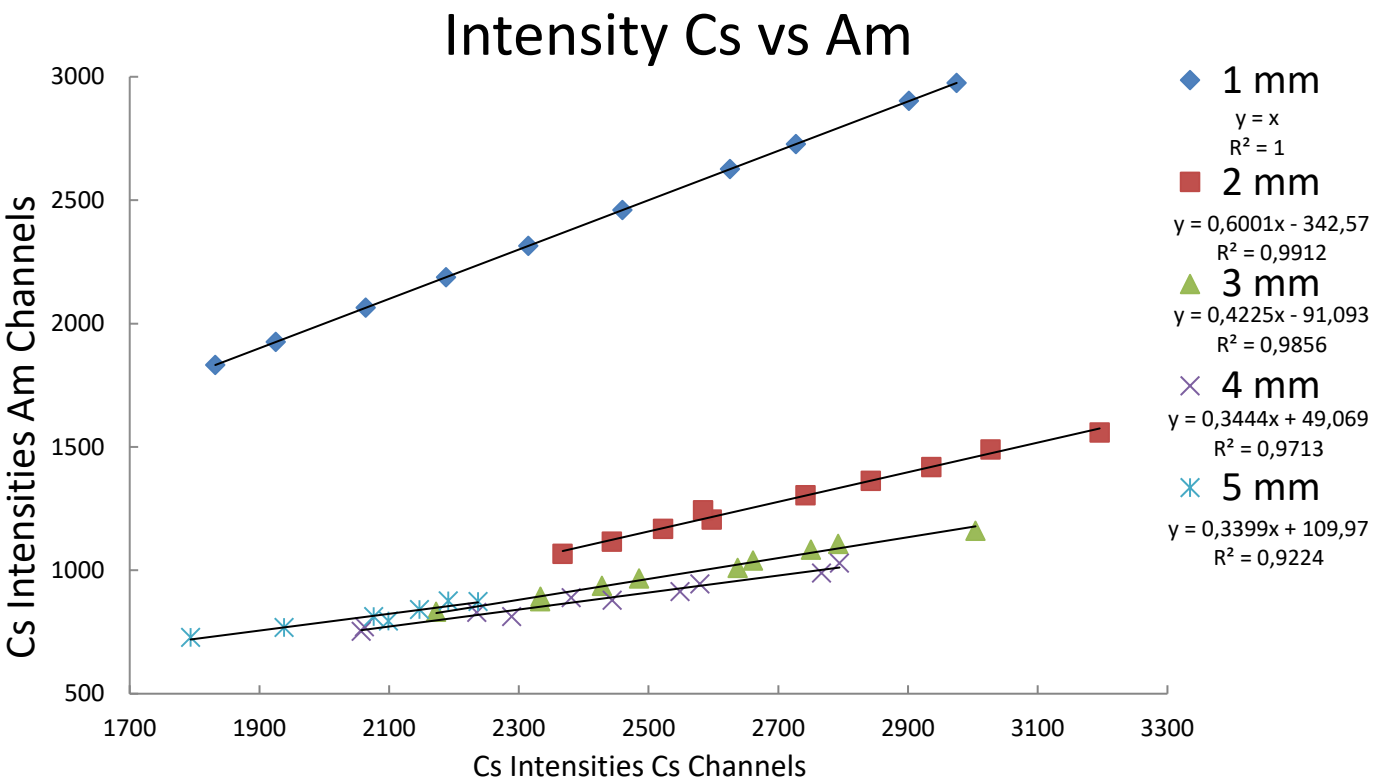

Figure 2: The 5 different linear functions are shown, representing the intensities measured when covering the emitter with brass (ranging from 1 mm to 5 mm).

The results shown in figure 2, presents the 5 linear functions, where each line are the measured intensities when the emitter was covered with 1 to 5 mm brass. The values of 4 mm have the lowest intensity values, which means that for this case, the intensities of Cs has been the most adsorbed. Therefore, we have chosen to use the value of 0,3444 (the slope of the function) as the Compton scattering correction for the measured intensity values for Am. The correction has been made for the results that will be presented when using Am and Cs during measurements.

2.2. Results attenuation coefficient

Results when using Cs and Am are emitted

The following results are the intensities measured using 1 to 7 cuvettes (as explained in section 1). Table 1 represents the intensities of empty cuvettes, and table 2 the same cuvettes but filled with water. Using formula 1, the results of Cs and Am intensities of water are plotted separately in figure 3 and 4. The slope represents the attenuation coefficient. Note, that because of the stability of Am, the accuracy is higher in comparison to Cs.

Table 1. Intensity of empty cuvettes		
# of cuvettes	**Am**	**Cs**
1	23909,6	6315,7
2	23243,8	6293,2
3	22195,9	5778,4
4	21557,6	5657,8
5	20891,8	5610,9
6	20469,1	5682,8
7	19742,7	5461,0

Table 2. Intensity of water-filled cuvettes		
# of cuvettes	**Am**	**Cs**
1	19548,7	5517,6
2	15520,5	4325,1
3	12484,2	4325,1
4	9893,8	3733,2
5	7889,7	3310,5
6	6289,3	2845,4
7	5061,7	2533,9

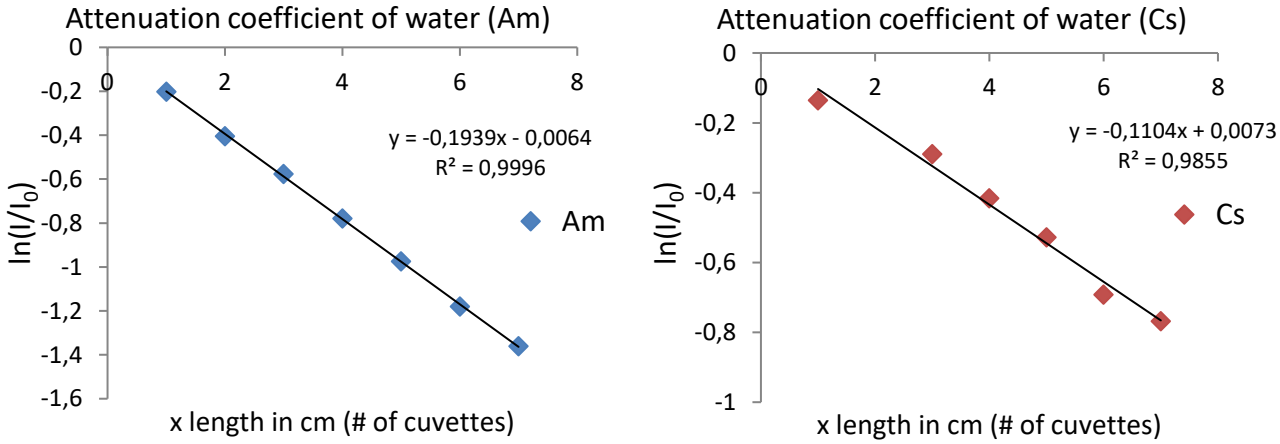

Figure 3: The resulting linear function found when plotting the $\ln(I/I_0)$ of the measured intensity over the reference intensity. The slope of the linear function is the attenuation coefficient for Am (left) and Cs (right).

The same procedure has been implemented when calculating the attenuation coefficient of the solution at various saturation levels (from 4% to 14%). The intensities of each concentration in the cuvettes, for both Cs and Am are given in section 2.3.

2.3. Solution cuvettes ($MnCl_2$)

Concentration: 4% w/w ratio

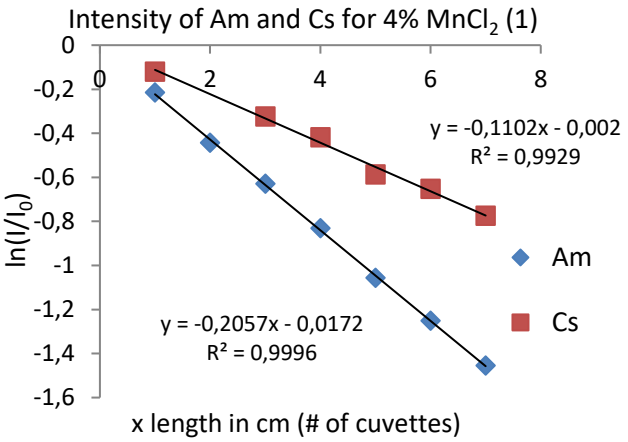

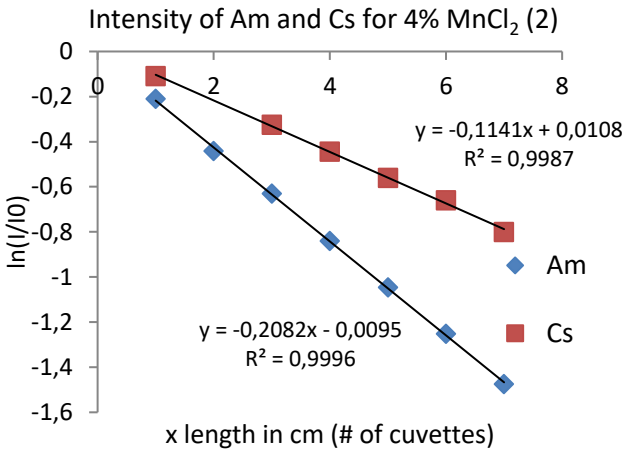

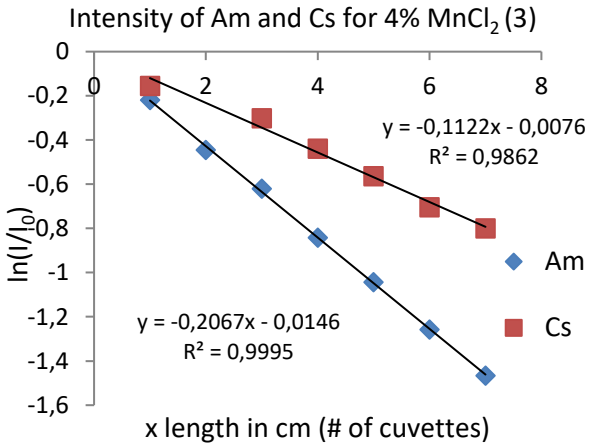

Concentration: 6% w/w ratio

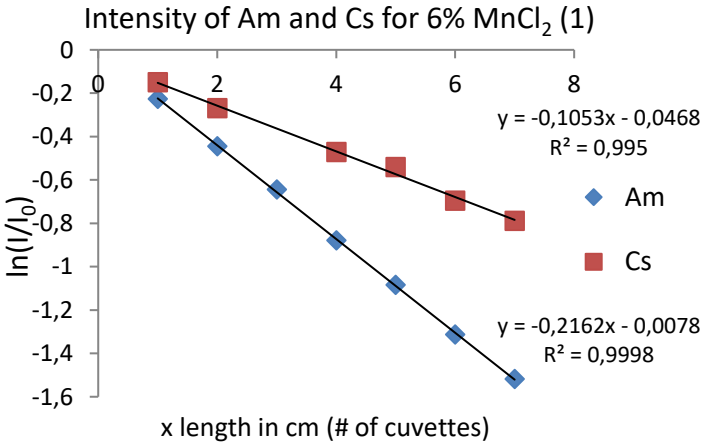

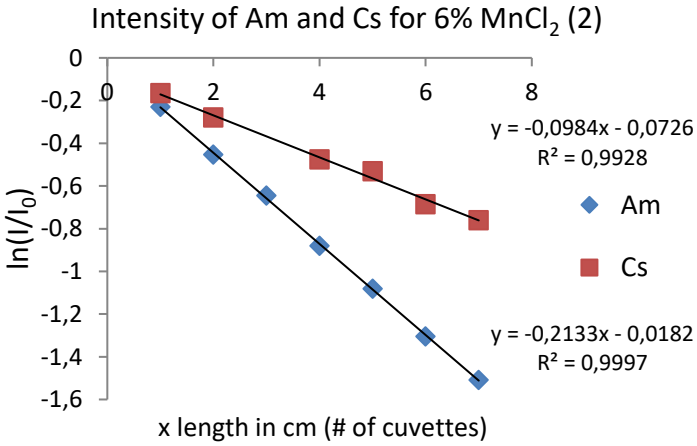

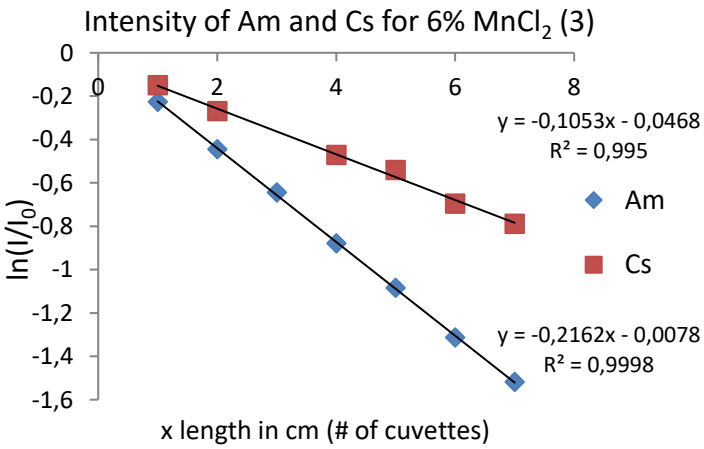

Concentration: 8% w/w ratio

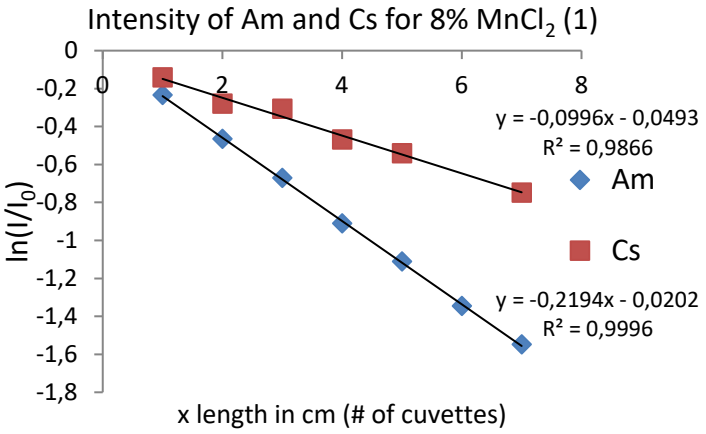

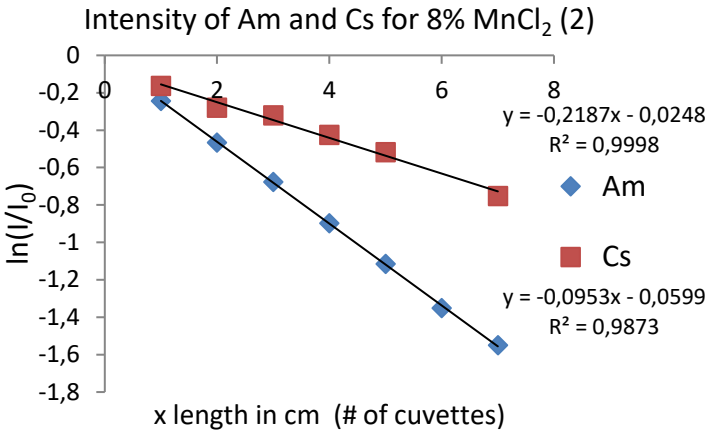

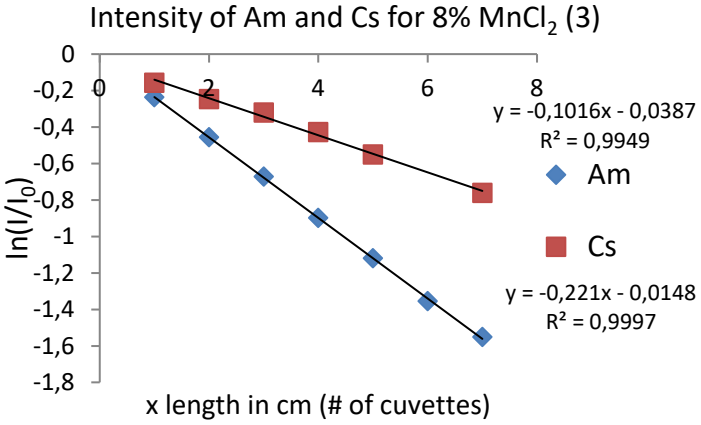

Concentration: 10% w/w ratio

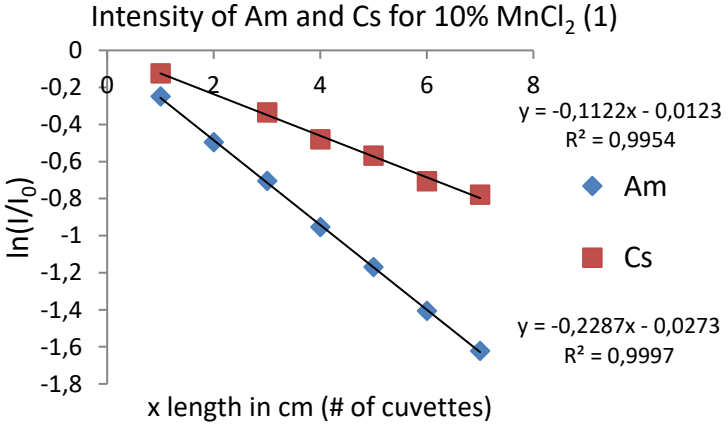

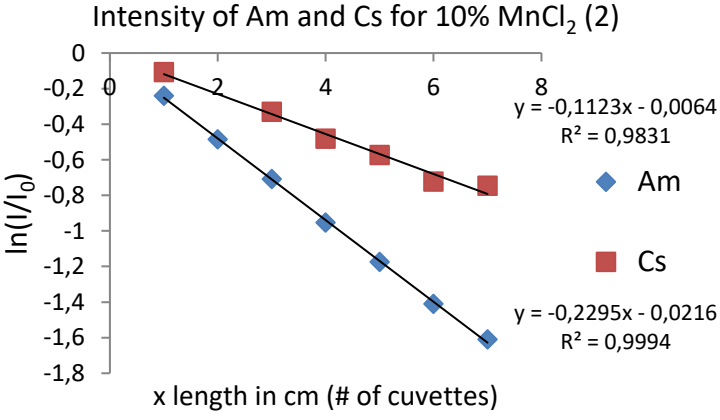

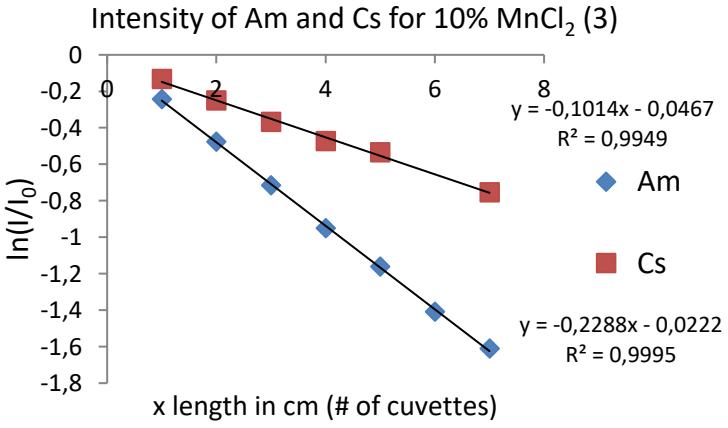

Concentration: 12% w/w ratio

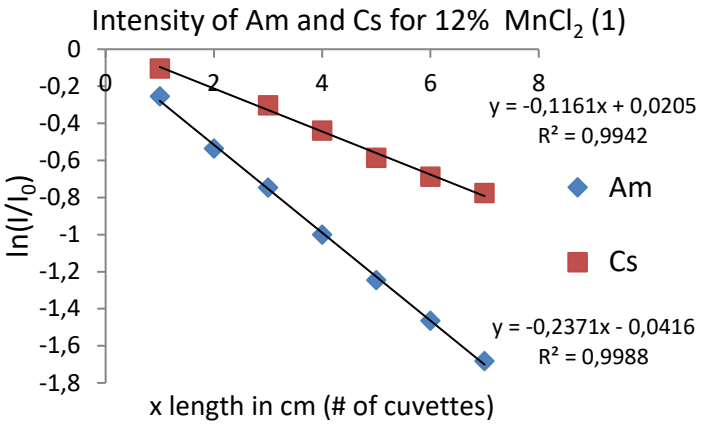

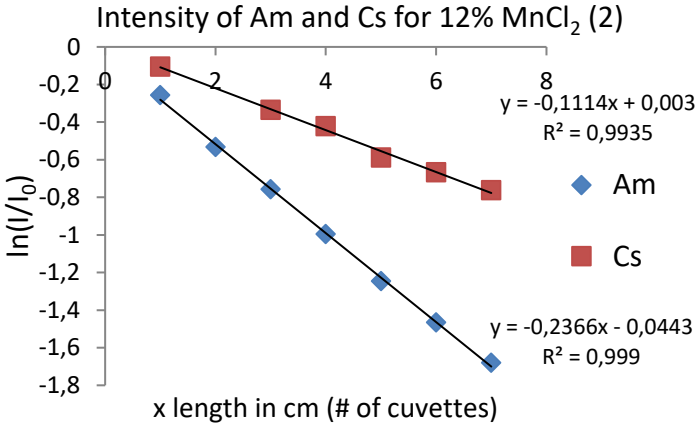

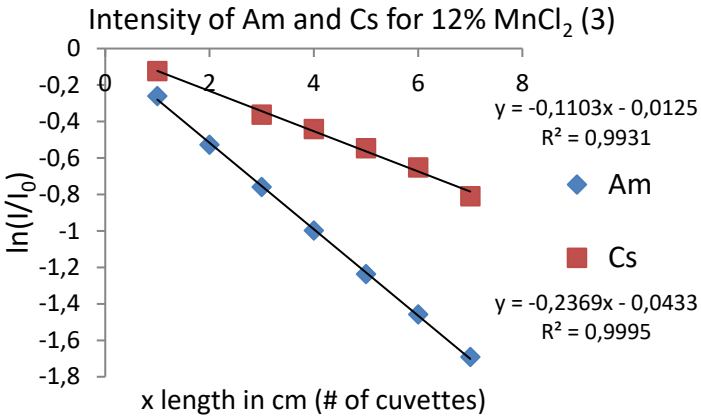

Concentration: 14% w/w ratio

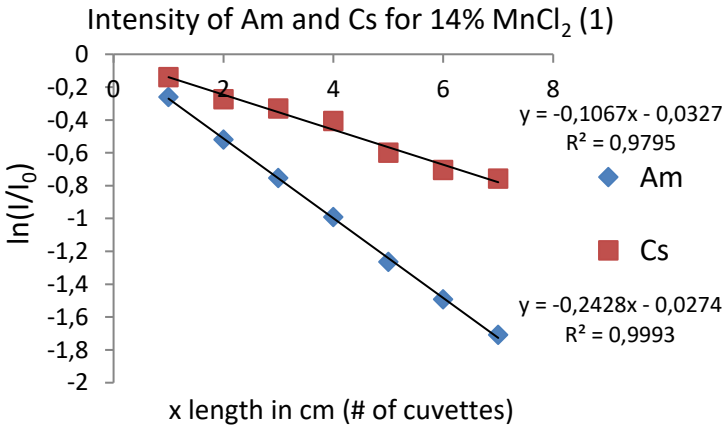

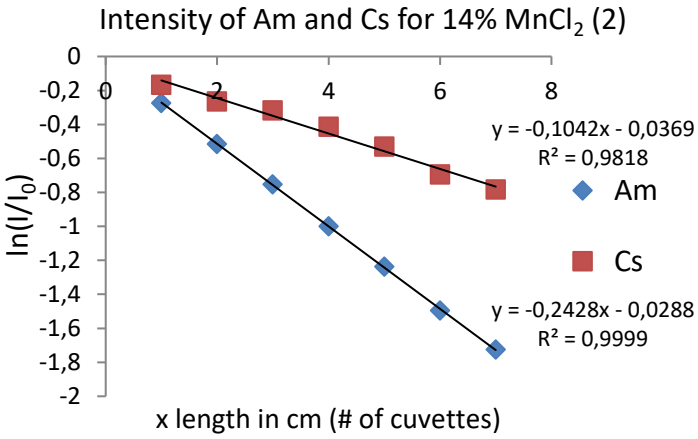

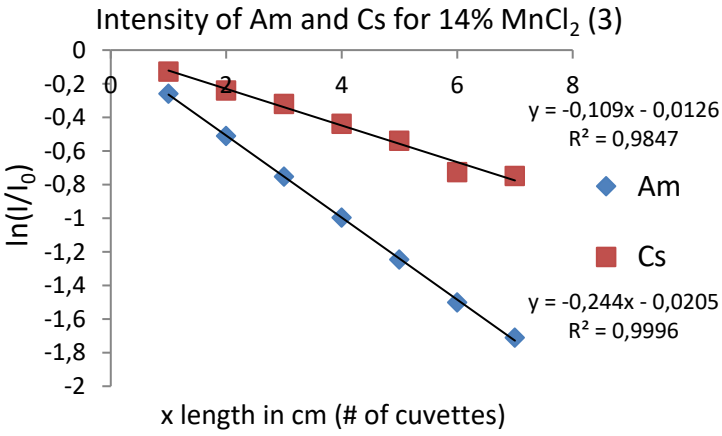

Appendix D

Saturation calculations

First of all, the average porosity is determined. This is calculated as;

$$\varphi_{av} = 1 - \frac{p_b}{p_d} = 1 - \frac{1{,}6098}{2{,}65} = 0.39$$

Saturation has been calculated using the formula: $\mathbf{S = \frac{X_w}{2 - X_s}}$ [1]

Where X_w, is the length of water in the column, which under saturated conditions in this case would be 2 times the porosity, which is 2*0.39 = 0.78 cm. X_s would be the length of the sand, which under saturation is 2-0.78 = 1.22 cm. Under unsaturated conditions, the saturation should be measured, in order to estimate it accurately. Therefore, the gamma-ray is used, in order to find X_w. Using the following calculations;

$$I_1 = I_0 e^{-\mu_s x_s^1 - \mu_w x_w^1} \quad [2]$$

$$I_2 = I_0 e^{-\mu_s x_s^1 - \mu_w x_w^1} \quad [3]$$

Dividing I_1 *by* I_2 gives: $\mathbf{\ln\left(\frac{I_1}{I_2}\right) = \mu_w(x_w^2 - x_w^1)}$ [4]

$X^1_w = 2*\phi_{av}$, because the column is 2 cm wide. X^2_w can be calculated using formula 2.

Appendix E – Results BTC's

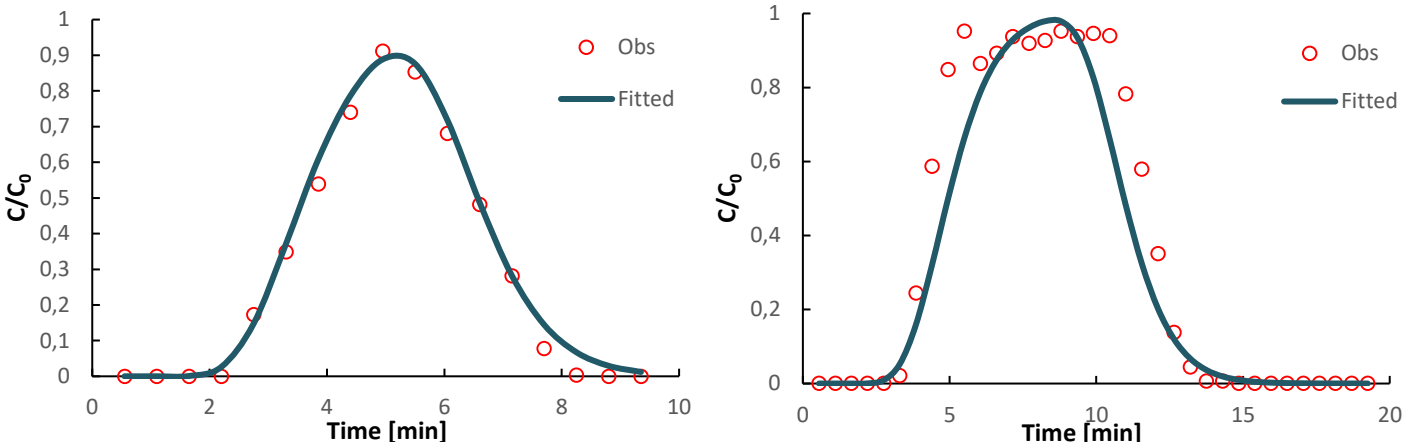

Figure 1. Breakthrough curves under saturated condition (S_w=1) at one location (1.5 cm) from inlet. Flux 1 = 2.685 cm min^{-1} (left) and Flux 2 = 1.259 cm min^{-1} (right). Points indicate observation data, lines indicate fit by ADE-model in CXTFIT

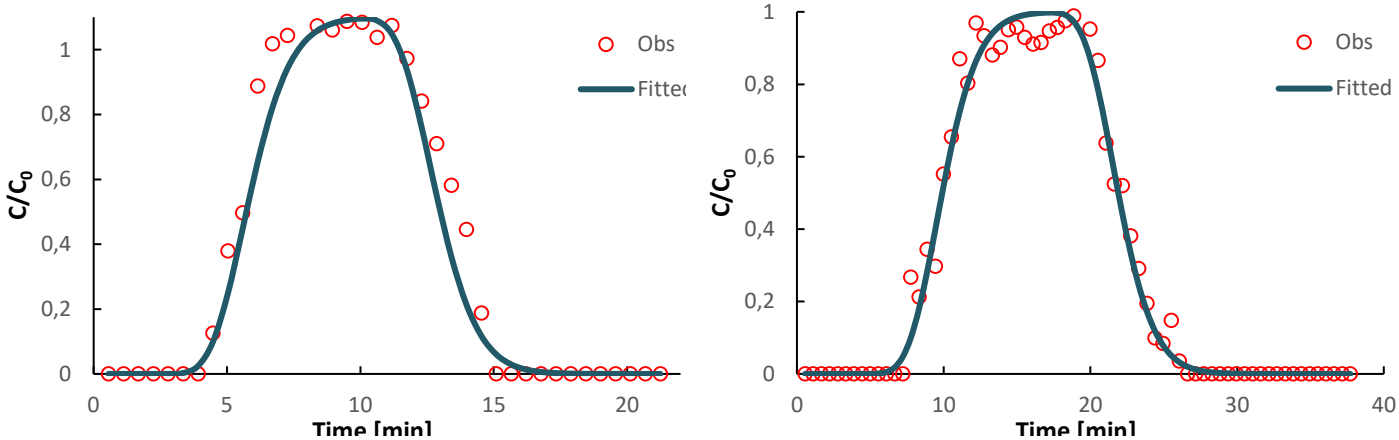

Figure 2. Breakthrough curves under unsaturated condition (S_w=0.78 and 0.69) at one location (1.5 cm) from inlet. Flux 1 (S_w = 0.78) = 1.069 cm min^{-1} (left) and Flux 2 (S_w = 0.69) = 0.664 cm min^{-1} (right). Points indicate observation data, lines indicate fit by ADE-model in CXTFIT

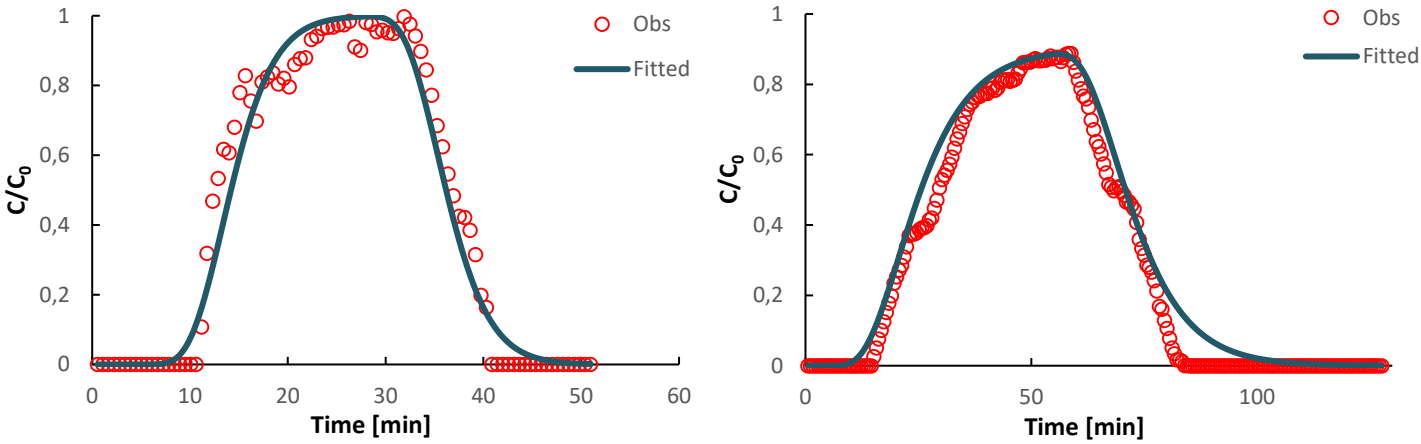

Figure 3. Breakthrough curves under unsaturated condition (S_w=0.6 and 0.51) at one location (1.5 cm) from inlet. Flux 1 (S_w = 0.6) = 0.378 cm min^{-1} (left) and Flux 2 (S_w = 0.51) = 0.112 cm min^{-1} (right). Points indicate observation data, lines indicate fit by ADE-model in CXTFIT

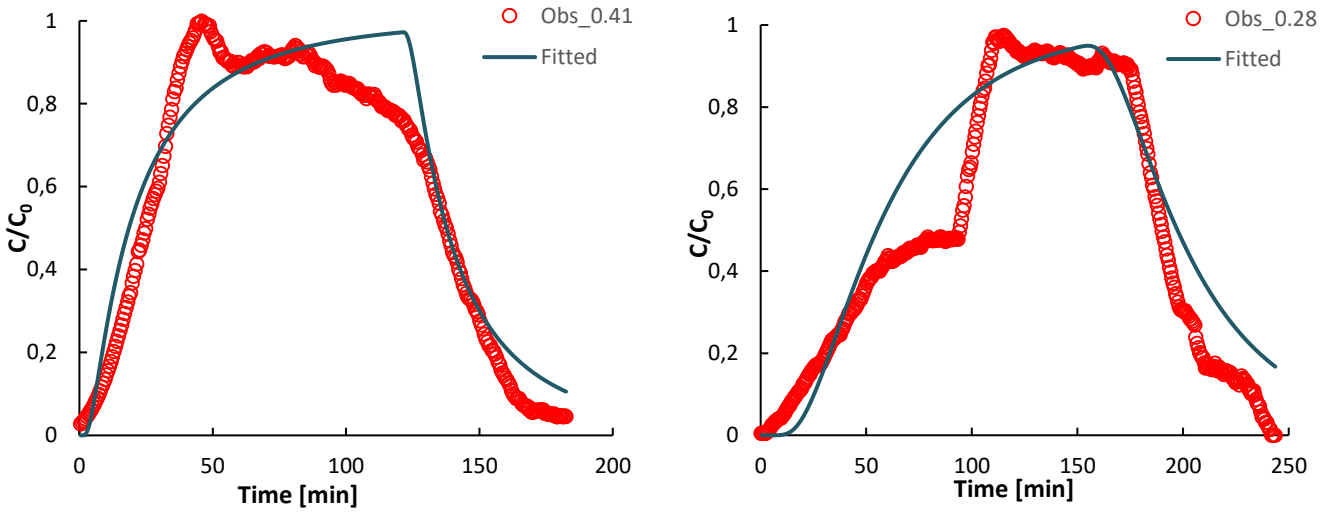

Figure 4. Breakthrough curves under unsaturated condition (S_w=0.41 and 0.28) at one location (1.5 cm) from inlet. Flux 1 (S_w = 0.41) = 0.075 cm min^{-1} (left) and Flux 2 (S_w = 0.28) = 0.023 cm min^{-1} (right). Points indicate observation data, lines indicate fit by ADE-model in CXTFIT